Sigma Journal of Engineering and Natural Sciences
Web page info: https://sigma.yildiz.edu.tr
DOI: 10.14744/sigma.2026.1992

Research Article

Formation and analysis of thermal images for infrared radiations from top of the atmosphere

Usama Ayub YOUSUFZAI[1,2*], Muhammad Jawed IQBAL[1], Faisal AFRIDI[1]

[1]Institute of Space Science and Technology, University of Karachi, Karachi, 75270, Pakistan
2 Department of Physics, NED University of Engineering & Technology Karachi, 75270, Pakistan

ARTICLE INFO

Article history
Received: 30 September 2024
Revised: 02 December 2024
Accepted: 15 January 2025

Keywords:
Filtering Techniques; Infrared Radiations, Interpolating Techniques, IR Thermal Images, Top of The Atmosphere

ABSTRACT

This research focused on the designing and analysis of thermal images with different interpolating techniques and proposed three competitive Filtering algorithms for infrared radiations from the Synoptic top of the atmosphere and surface fluxes & clouds - SYN Ed4A, which is the data product of Clouds & the Earth's Radiant Energy System (CERES) used for collection of daily ten-year data for infrared radiations. This kind of study carried out first time in Pakistan. This work aims to enhance our comprehension of climate and weather systems, facilitated by the generation and analysis of thermal images capturing infrared radiation from the upper atmosphere. State of the art techniques in Modern technologies for creating and analyzing thermal images of infrared radiation from the upper atmosphere include complex calibration procedures, machine learning algorithms for improved image processing, and modern satellite sensors. This work is an attempt to investigate the quantification of infrared flux using different interpolating techniques and filtering algorithms. We discussed that how we interface MATLAB to data. As well as we also discussed about the generation of thermal maps and thermal images through MATLAB with different interpolating techniques. We will also discussed about filtering techniques for thermal images and proposed three different filtering algorithms. It also analyzed for the characterization of thermal images, which generated from different interpolated transformation and digital filtering techniques. We have used different techniques to devise digital filters and enhance the resolution of thermal images after that recognized and characterized thermal images of infrared radiations. We can use these algorithms for other different purposes based on the regular datasets like Data integration and fusion, Mitigating atmospheric inferences high resolutions image techniques, Long-term data consistency, advanced image processing algorithms etc.

Cite this article as: Yousufzai UA, Iqbal MJ, Afridi F. Formation and analysis of thermal images for infrared radiations from top of the atmosphere. Sigma J Eng Nat Sci 2026;44(1):465–477.

***Corresponding author.**
*E-mail address: usamaayub@neduet.edu.pk

This paper was recommended for publication in revised form by Editor-in-Chief Ahmet Selim Dalkilic

INTRODUCTION

The Earth and its atmosphere emit infrared radiation into space, which results in infrared flux rising from the top of the atmosphere. This radiation has a significant role in regulating the temperature of planet, as it is a component of the energy balance of the climate system [1].

The following are the primary sources of infrared radiation from the upper atmosphere:

Earth's Surface: Solar energy absorbed by the Earth's surface and reemitted as infrared radiation. One of the main sources of the infrared flux originating from the top of the atmosphere is this thermal radiation [2].

Atmospheric Gases: Water vapor, carbon dioxide, and methane are among the gases that emit infrared radiation from the Earth's atmosphere [3]. These gases add to the total flux of infrared radiation originating from the top of the atmosphere by both absorbing and reemitting thermal radiation.

Clouds: The emission of infrared radiation from the upper atmosphere significantly influenced by clouds. Their kind, altitude, and thickness determine how much they contribute to the total infrared flux [4]. They have the ability to both reflect and absorb thermal radiation.

The quantity of infrared flux originating from the upper atmosphere is a crucial component in comprehending the energy balance of the Earth and the worldwide climate [5]. It is also crucial for many other applications, such as climate modeling, weather forecasting, and satellite remote sensing. Furthermore, variations in the quantity and distribution of infrared flux can have a major influence on Earth's temperature and climate, which is why atmospheric science and climate research must pay close attention to this field of study [6]. The Sun is a source of visible light, but it also produces infrared radiation, which is a component of the electromagnetic spectrum. Actually, the Sun emits nearly half of its total energy as infrared radiation [7].

With a surface temperature of about 5,500 degrees Celsius, the Sun is a highly hot object that produces infrared radiation. The Sun emits radiation, including infrared radiation, as result of its extreme heat [8]. Telescopes and satellites are among the devices that may detect this energy, which carried through space as electromagnetic waves [9]. There are several uses for the Sun's infrared energy. It can used, for instance, to investigate the makeup and characteristics of the Sun's atmosphere and surface as well as the solar wind, a stream of charged particles that emerges from the Sun continuously [10]. The Sun's infrared radiation also has a significant impact on Earth's weather and climate [11]. It is the primary energy source for weather patterns and air circulation in the Earth's climate system. The Earth's surface and atmosphere absorb infrared radiation from the Sun, which then sent back into space as thermal radiation in the form of infrared waves [12]. The Earth's energy balance depends heavily on this thermal radiation, which also plays a major role in regulating the planet's temperature and climate [13].

All of the CERES (Clouds and the Earth's Radiant Energy System (CERES) Energy Balanced and Filled (EBAF) Top-of-Atmosphere (TOA)) footprints (20 km nominal resolution) within the specified temporal or spatial domain used to calculate the all-sky scene, also referred to as total [14]. There are a number of observations from 2011 to 2020. Depending on the product, Clear-Sky scenario offers multiple algorithms: ERBE-like, Energy Balanced and Filled (EBAF), Single Scanner Footprint TOA/Surface Fluxes and Clouds (SSF) [15]. Climatic zonal Longwave (LW) criteria and suitable Shortwave (SW) thresholds used by the Earth Radiation Budget Experiment (ERBE) scene id algorithm (Identifier) to select the clear-sky scene from CERES footprints that were inferred as clear. In this instance, the collection of observations dates back to 2011 to 2020.

For the regions without clouds, we were able to gather a set of observations for TOA infrared flux -All sky and TOA infrared flux -Clear Sky. The observations from CERES_EBAF-TOA_Ed4.1 span the years 2011 to 2020.

Data integration and fusion, mitigating atmospheric inferences, high resolution image techniques, long-term data consistency, advanced image processing algorithms, modeling thermal emission sources, impact of atmospheric dynamics, and real-time data processing are just a few of the gaps that this study will help us bridge [16].

The reason behind this study only for our understanding of climate and weather systems has advanced significantly due to the creation and analysis of thermal pictures for infrared radiations from the top of the atmosphere [17]. Notwithstanding the difficulties, multidisciplinary research and continuous technical development are improving the precision and usefulness of thermal imaging data, greatly advancing meteorology and climate science [18]. State of the art techniques in Modern technologies for creating and analyzing thermal images of infrared radiation from the upper atmosphere include complex calibration procedures, machine learning algorithms for improved image processing, and modern satellite sensors [19,20]. These developments make it possible to monitor atmospheric conditions with great precision and accuracy, which is essential for weather forecasting and climate science.

Practical Aspect

A precise methodology will followed in order to practically identified, how the atmospheric data retrieved from the NASA portal used to generate the conclusions for this research. Initially, the Earth's Radiant Energy System (CERES) Ordering Tool on NASA's Clouds would use to retrieve all available infrared flux data [21]. To effective prediction the radiative properties of the Earth, this data would be essential. Then, using this information, we would calibrate infrared sensors to correspond with the particular air conditions that noted during the data gathering [22]. The infrared radiation data would be processed using algorithms that take into consideration the atmospheric factors that retrieved from NASA's database to create the thermal images [23]. This

ensures that the images accurately represent the thermal emissions from the top of the atmosphere. The results would analyzed to identify trends or anomalies in infrared radiations [24]. This approach allows for a more accurate interpretation of the thermal images, linking observed radiation patterns directly to atmospheric conditions.

MATERIALS AND METHODS

Study Location and Data Collection

The required data sets have recorded from NASA website termed as Clouds and the Earth's Radiant Energy System (CERES) Energy Balanced and Filled (EBAF) Top-of-Atmosphere (TOA) Edition-4.0 and 4.1 Data Products [25]. Cloud ERES_EBAF_Ed4.1 Data Quality Summary, Investigation: CERES and Data Product: EBAF, Set of observations: Terra-MODIS (Instruments: CERES-FM1orCERES-FM2) and Aqua-MODIS (Instruments: CERES-FM3 orCERES-FM4, set of observations Version: Edition 4.1. The scope of the CERES Ordering Tool was to provide developers and users with a fast and easy way of accessing CERES Data by means of Visualization (or browsing) and Subsetting (or ordering) [26]. Spatial resolution was set to regional of Pakistan (global grid) with the coordinates 60.83333 W, 77.83333 E, 37.08333 N, and 23.583 S.

After downloading the file from the CERES ordering tool, the file opened in the software "Panoply". Panoply is a software platform that is compatible with desktop computers running on Windows, Macintosh, Linux, and other operating systems. A compatible version of Java 11 or later must installed on the computer to use the platform [27]. Here, Panoply used to extract a large amount of data in an Excel CSV file. The time parameter was not in the readable format for CSV. We have generated it using data transformation techniques for each year [28]. The generated date divided from year to months or quarters even we have divided it into days. By using data analytics approach, we have created pivot table and applied aggregation functions to find average yearly and monthly frequency distribution for data.

Software and Programming

In this section we will discussed the programming scripts written in MATLAB. For designing of thermal maps, a program script will initialize the data and it reads the data. After read and initializing the data and all parameters, we set 64 pixels data from 4×16 array. It outputs from Row-0 to Row-3. Each row consisting eight pixels, referenced from Col-0 to Col-15. The data starts from pixel-0 of Row-0 to pixel-15 of Row-0, then pixel-0 of Row-1 to pixel-15 of Row-1, this process continue up to the Row-3. Until, all 64 pixels data sent. It is not efficient to acquire 4×16 array data with separated rows. Through programming, we have convert 4×16 into 1×64 array as single frame to speed up data processing in MATLAB. After taking temperature values in 1×64, program will continue and take another frame. Otherwise, we will initialize again and start operation from the beginning.

Through MATLAB, we construct raw thermal images from data acquired in 1×64 frames. As well as this section describes enhancement and filtering techniques through MATLAB programming.

Enhancement of thermal images

Figure-1 shows the program flow for the construction and enhancement of thermal images for infrared radiations. As shown in figure, first MATLAB will interface with data. After interfacing, set all configuration values related to data as well as related to MATLAB. After setting all configuration values, an empty matrix of 4×16 created. MATLAB starts reading the data which coming from infrared in 1×64 array, as shown in Figure-2. Here, we set a

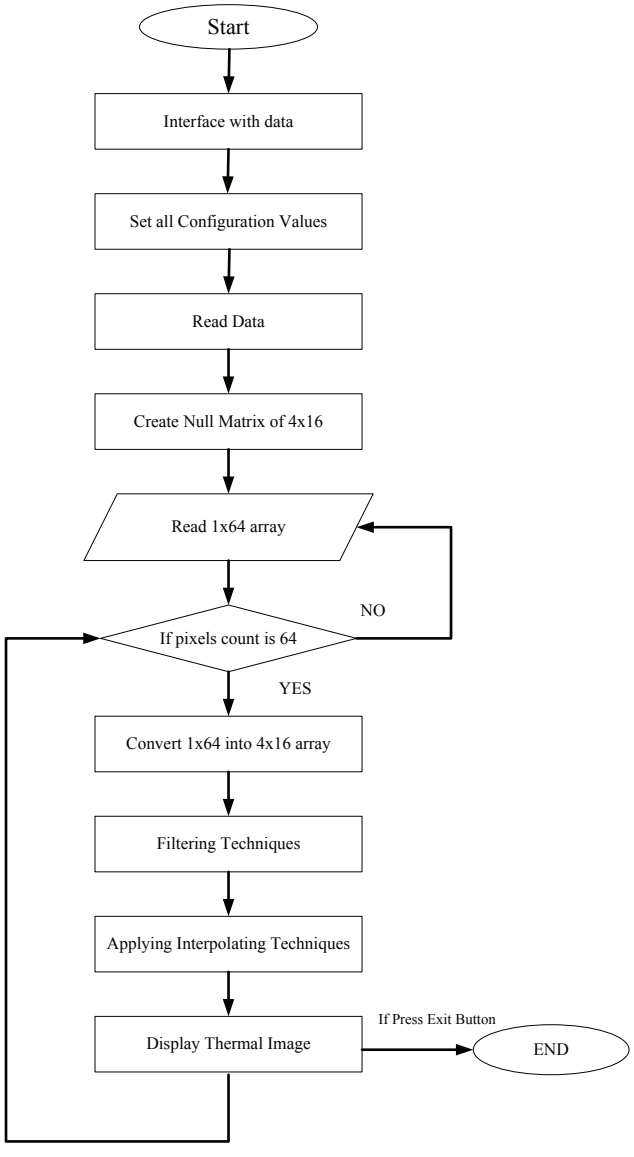

Figure 1. Program flow for the construction and enhancement of thermal maps.

condition that if interfacing system gives us 1×64 array, so, the program will execute further. Otherwise, take another next frame and so on [29]. After taking 1×64 array, convert this array again into 4×16, as shown in Figure-3. For graphical representation 'bargraph' plotting techniques has been used. As shown in Figure-4, we have used view command for setting the thermal array bar top on the front of the screen for using as a thermal screen. Text command has

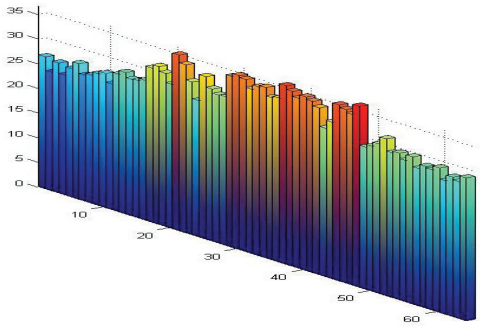

Figure 2. 1×64 Thermal pixels.

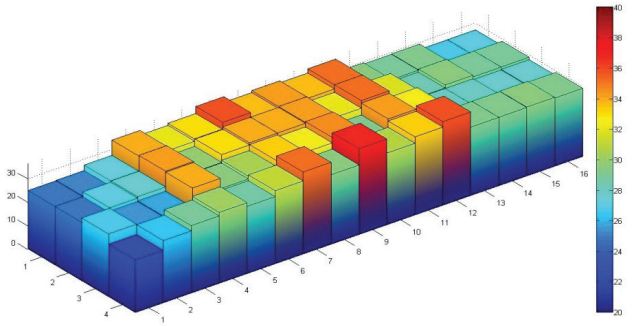

Figure 3. 4×16 Thermal pixels.

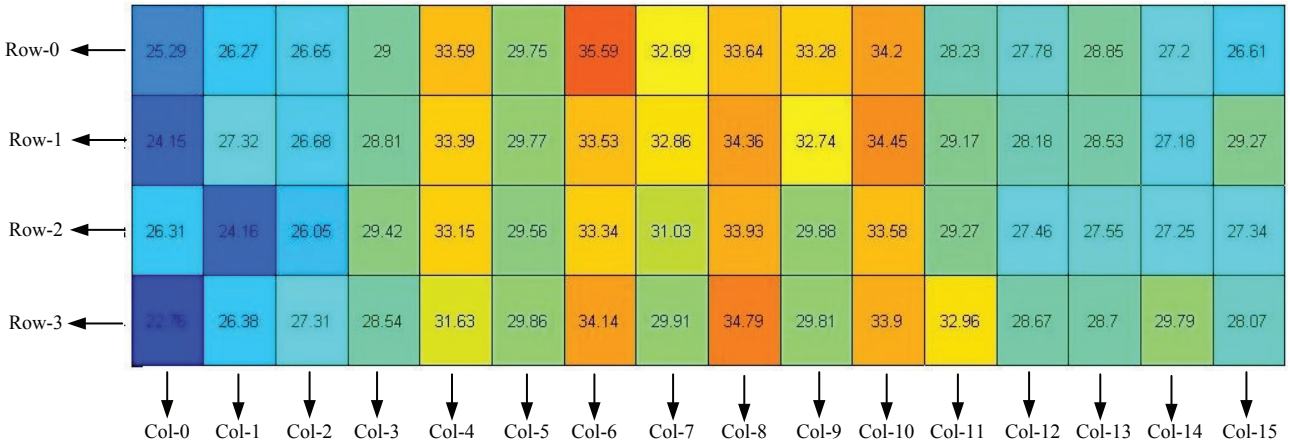

Figure 4. 4×16 Thermal Pixels with values.

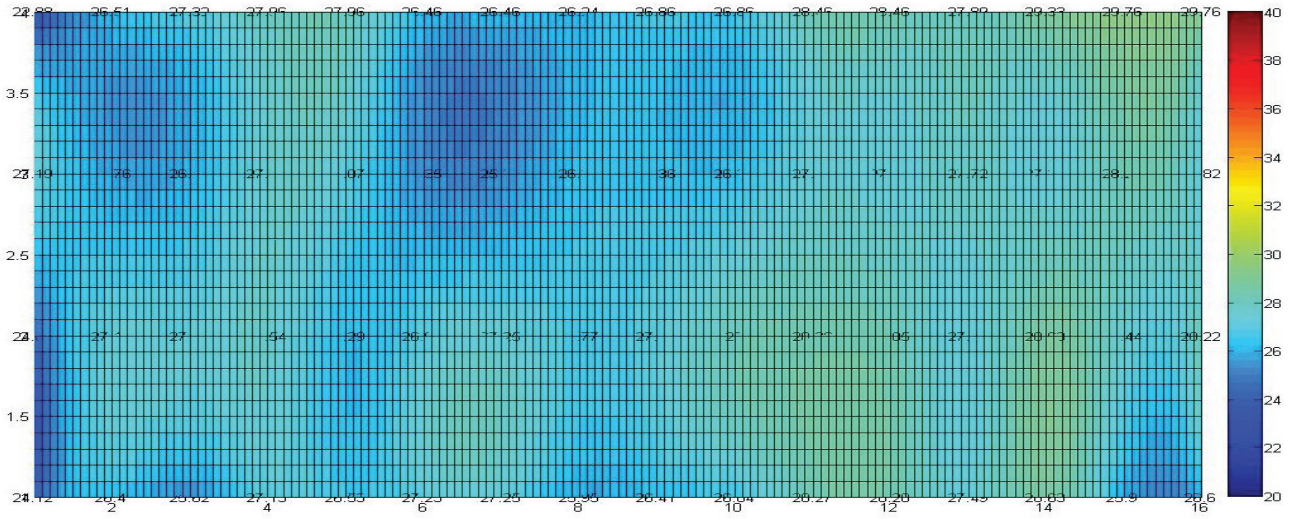

Figure 5. Thermal Image after enhancement in 31×151 array.

been used for display the values on each n every pixel of array. Range of the color bar is set from 20°C to 40°C by using command 'caxis' [7, 30].

Representation from colors

There are many color maps available in MATLAB e.g. Jet, HSV, Hot, Cool, etc. Here, we have used Jet color map, because the Jet color map is suitable for thermal mapping, because the in red color mapping represent the highest temperature and the dark blue color represents the lowest temperature [7]. The Jet based on the variation of HSV color map. The Jet designed by The National Center for Supercomputer Applications (NCSA) [8].

After generation of raw thermal image, interpolating techniques have used to enhance the thermal images, as shown in Figure-5. For this purpose, we have used surface command in place of bar graph and convert 4×16 array into 31×151 with the help of 'meshgrid' command [8]. For interpolating techniques, we have use 'interp' command. Four different methods of interpolation have compared, which will discussed in the next section. At the end, different filtering techniques for the elimination of the noise factor in the thermal images, has utilized [31]. The filtering techniques will discussed later.

Interpolating Techniques

Figure 6a shows the interpolation using nearest neighboring method. In this type, image will interpolate with the help of nearest cell. Comparatively this interpolation technique provide worst image and we cannot justify and analyze this image. The main disadvantage of nearest is the slow speed, due to which poor quality image have generated. Figure 6b shows the thermal image coming from linear interpolation method. According to mathematics, the curve fitting method with the help of linear polynomial known as linear interpolation [9, 10].

If we compare nearest and linear, the interpolated result from linear is much better than nearest method. Figure-6(c) shows the thermal image using cubic method. In this type of interpolation, pixels joined with respect to cubic polynomial. The speed is also much better than last two methods. This image is almost identical to the interpolated

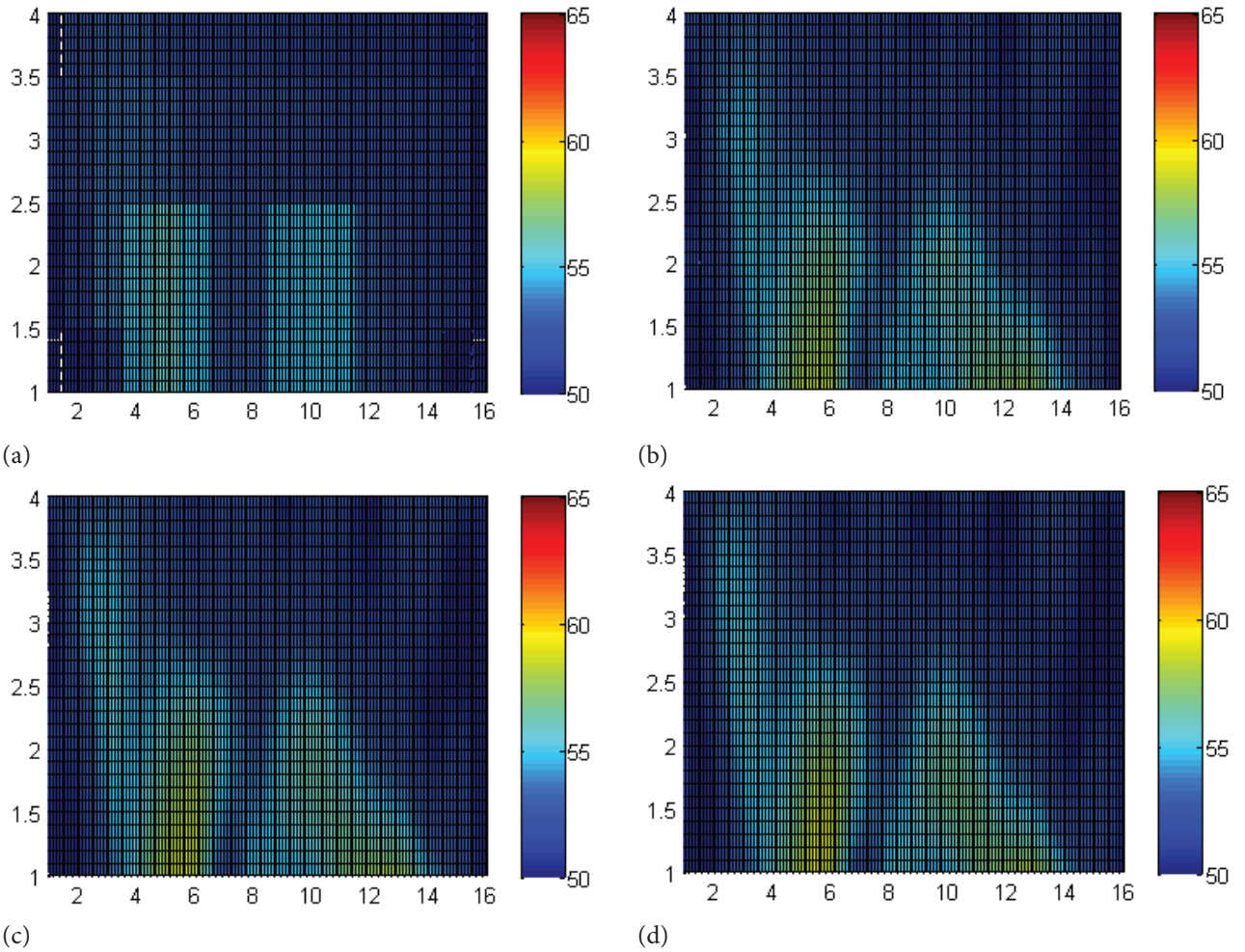

Figure 6. Thermal Image after using nearest, linear, cubic and spline interpolation.

image applying linear method. There is a difference, If we see in both the figures, the gaps between the pixels in Figure-6(c) is much clear than Figure-6(b). Figure-6(d) shows the thermal image using spline. The interpolation based on piecewise polynomial called as spline interpolation. Spline is coming from term elastic ruler. This type of interpolation preferred than others due to the interpolation error is much less. If we compare Figure-6(d) with others, so the thermal image generated from spline is much better than others. The noise factor is also very less as compare to other's thermal images.

Digital Filtering Techniques

In this paper, we focused on two already devised digital filters, which are median and conservative filter. Then focus on proposed Modified Conservative Filter (MCF) in three different inferences and compare the results of all three modified digital filters with each other as well as with conservative and median filter [11,12].

The median filter

The median filter used to remove noise from any signal or image. Median filtering technique is widely used in image processing and it is best for removing salt and pepper noise [10,13,14]. The Median filter is not suitable here. As we see in the Figure-7(a) the overall result of thermal image is poor and the image is not clear; we have a completely blurred image.

The conservative filter

In Conservative filter, generally the neighboring pixels of each n every pixel are select. In the next step, it finds minimum and maximum values in neighboring pixels. If the value is greater than maximum pixel value, the center pixel will be set at maximum value. If the value is less than the minimum pixel value, the center pixel will be set at the minimum value [14]. Figure-7(b) shows the thermal image after application of Conservative filter. Image becomes more improved. After this, we modify conservative filter into three different ways.

MCF-1

Figure-7(c) shows the result of thermal image after modification in conservative filter called as MCF-1 (Modification in Conservative Filter-1). The significance of this is to improve the frequency resolution. It impact on FFT means by increasing the amount of data points prior to performing a Fourier transform (FFT), zero padding produces a finer frequency resolution [32]. This makes it possible to identify frequency components with greater accuracy, particularly in situations where the original data was sparse or the frequencies were tightly spaced [13]. For example, a signal with 256 points zero-padded to 512 points will provide a frequency resolution twice as fine as the original [33]. Adjusting the amount of zero padding can help achieve the desired frequency resolution without unnecessarily increasing computational load [34]. For this modification, it get the double zero padding at the edges. Its means that, add two rows of zeros at above and at below of the array also add two columns of zeros at the left most and right most at the thermal frame. Select eight neighboring pixels for each n every pixel and repeat the same process, which already discussed in conservative filter. After application of this MCF-1, the image becomes noisy.

MCF-2

Figure-7(d) shows the thermal image after another modification in conservative filter called as MCF-2 (Modification in Conservative Filter-2). The significance of this is to reduce the edge effect because the finite length of the filter and the signal might cause distortion of the signal's edges when it filtered [35]. By supplying a buffer of zeros around the original signal, zero padding reduces these edge effects and makes sure that the signal's crucial components not distorted throughout the filtering process [10]. This modification also adapted zero padding, but here, it selects only four neighboring pixels. Through this filter, the image becomes better as compare to Figure-7(c).

MCF-3

Figure-7(e) shows the resulted thermal image after another modification in conservative filter called as MCF-3 (Modification in Conservative Filter-3). For this modification, the zero padding will again double. Here, we select total 24 neighboring pixels for the process of each n every pixel and repeat the same process discussed in conservative filter. Due to double zero padding and selection of 24 neighboring pixels, the noise factor becomes much less as compare to other schemes. The significance of this is to improve computational efficiency because it is possible to apply the FFT approach, which is computationally efficient for such lengths, by zero padding to a length that is a power of two. As a result, filtering processes take less computer power and time, increasing process efficiency [14]. The image quality also increases because we consider maximum neighboring pixels.

Now, if we compare the thermal image result of Figure-7(a), (b), (c), (d) and (e). Figure-7(e) is much better and the noise factor is very less as compared to median and conservative filter. The median filter is not suitable here. If we compare all three modification in conservative filter, so the last one modification which shown in Figure-7(e) is suitable than others.

RESULTS AND DISCUSSION

If we compare the image results of Figure-8(a), (b), (c), (d) and (e), so we observe that the Median Filter and MCF-1 are not suitable for our purpose and gave false interpolated thermal response as compared to other filters. Median filter perform well in other purposes but here, Median filter could not work properly. Where, the image result after applying proposed MCF-3, MCF-2 and Conservative filter becomes

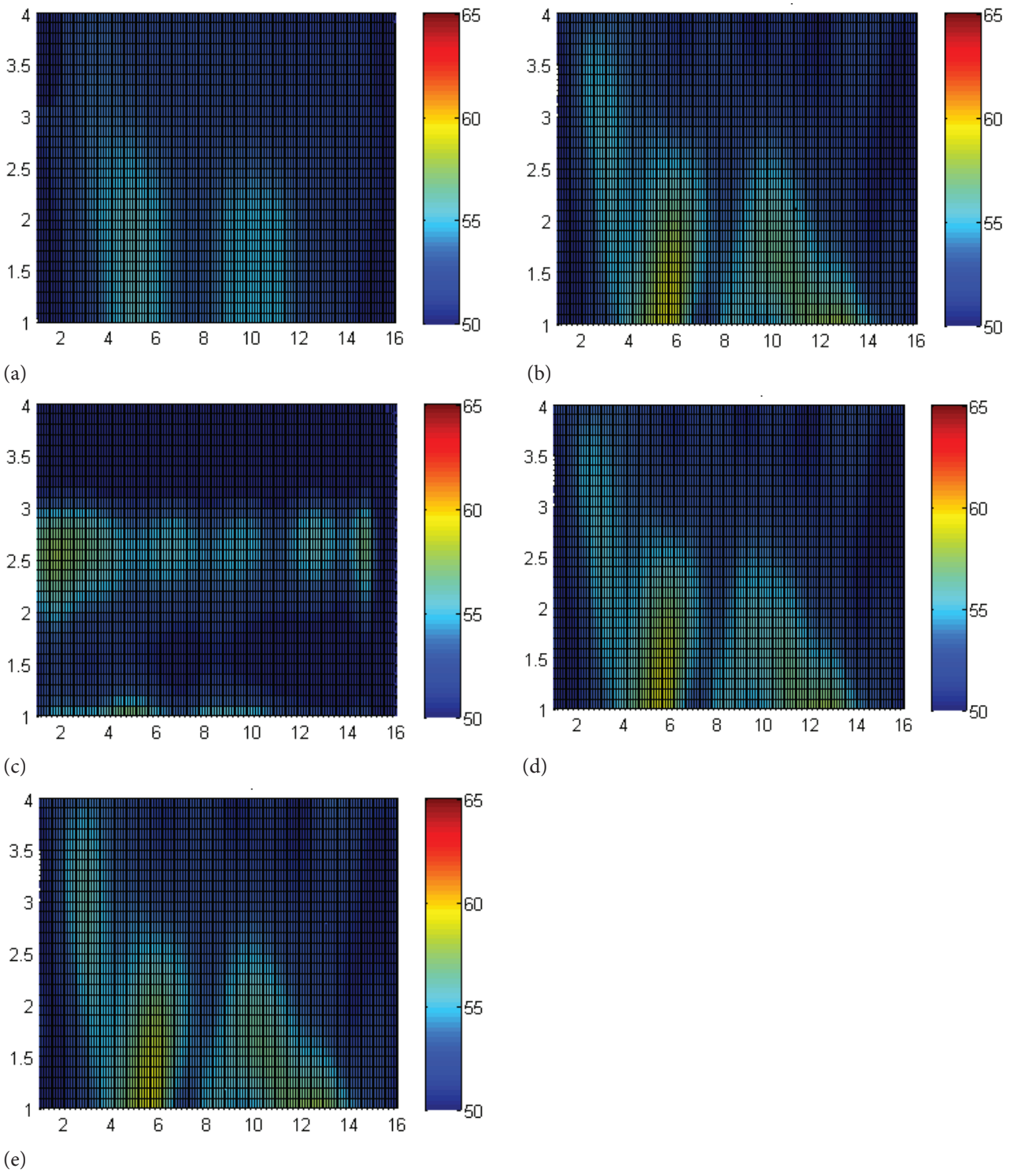

Figure 7. Thermal Image after using median, conservative, MCF-1, MCF-2 and MCF-3 filters.

good. In all these three filters, the proposed MCF-3 gives much better thermal contrast as compare to MCF-2 and Conservative filter. If we discuss about interpolating techniques, so the sp-line method gives much better and high quality images as compared to cubic, linear and nearest.

We are taking the data of infrared radiations and here we will select Row-27 of 31 interpolated rows for quantitative analysis. Figure-9(a), (b), (c), (d) and (e) shows the thermal response of interpolated-Row-27 (Interp-R27) of 31 rows of Figure-8(a), (b), (c), (d) and (e) respectively. Blue, Green, Red and Aqua color shows the response of the interpolating

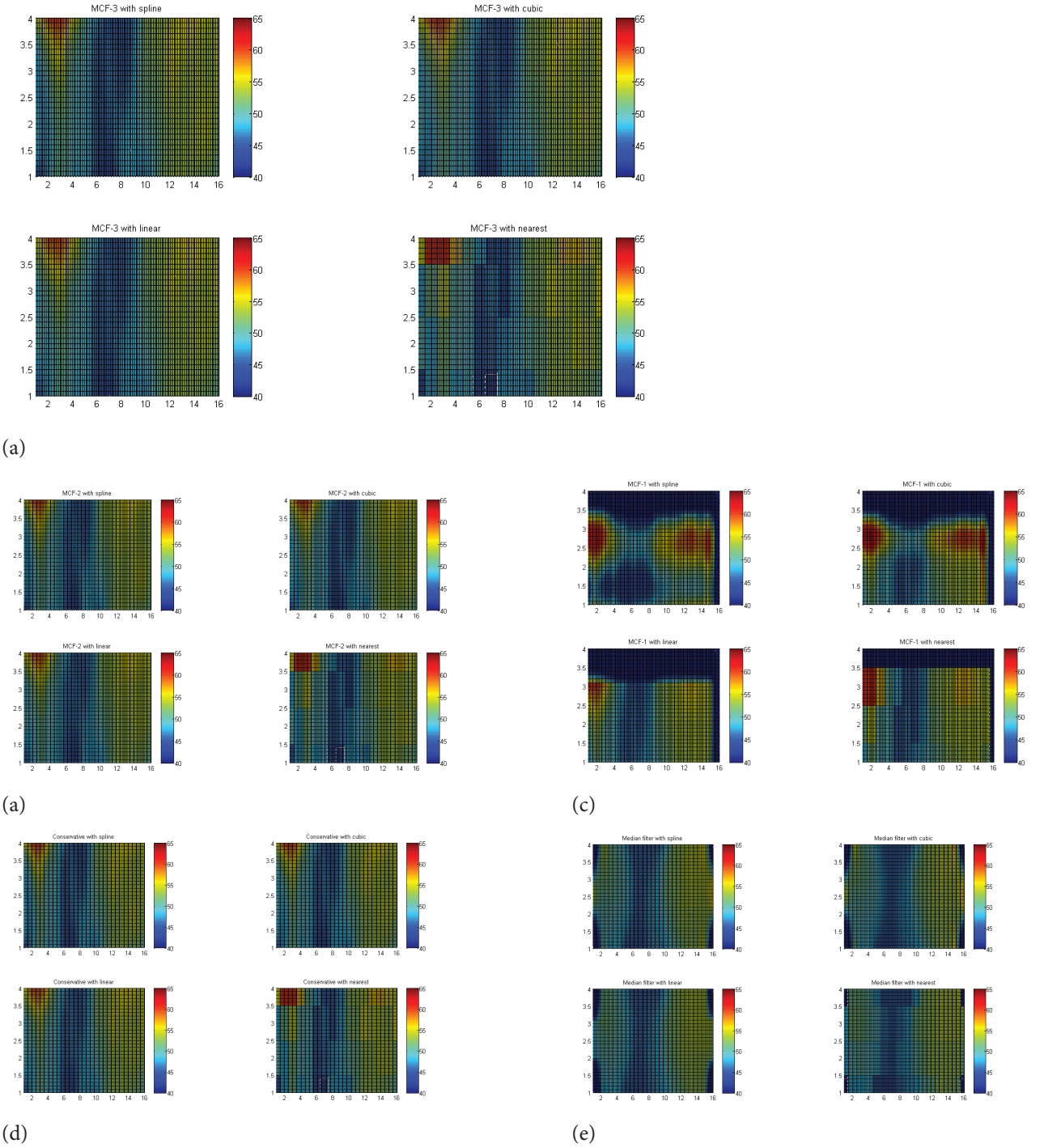

Figure 8. Thermal response of MCF-3, 2, 1, conservative and median filter with interpolations.

methods of Sp-line, Cubic, Linear and Nearest respectively. All the responses drawn graphically with the help of data and the interpolated pixels. Here, we can clearly see that proposed MCF-3 gives much better response comparatively where the Median and MCF-1 gives poor response.

Table 1 to Table 5 shows the extracted data from Figure-9(a) to Figure-9(e) respectively. In these tables, 'Min1' shows the first minima data values where 'Min2' shows the second minima data values. 'Max1', 'Max2' and 'Max3' show the maxima data values at the top. 'DF1' and 'DF2' show the contrasts values which are related to 'Min1-Max1' and 'Min1-Max2' respectively, where 'DDF1' shows the contrast related to 'DF1' and 'DF2' with all four interpolating techniques using MCF-3, MCF-2, MCF-1, Conservative and Median Filter separately. 'D1' and 'D2' also show the contrasts, which are relate to 'Min2-Max2' and 'Min2-Max3' respectively, where 'DDF2'

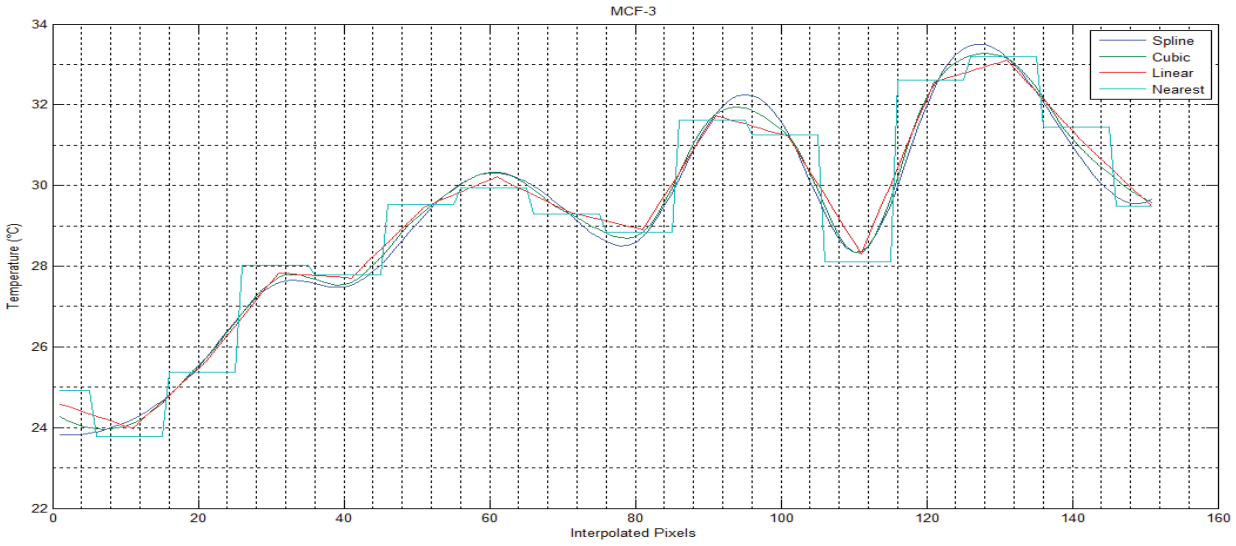
MCF-3
Spline
Cubic
Linear
Nearest
Temperature (°C)
Interpolated Pixels

(a)

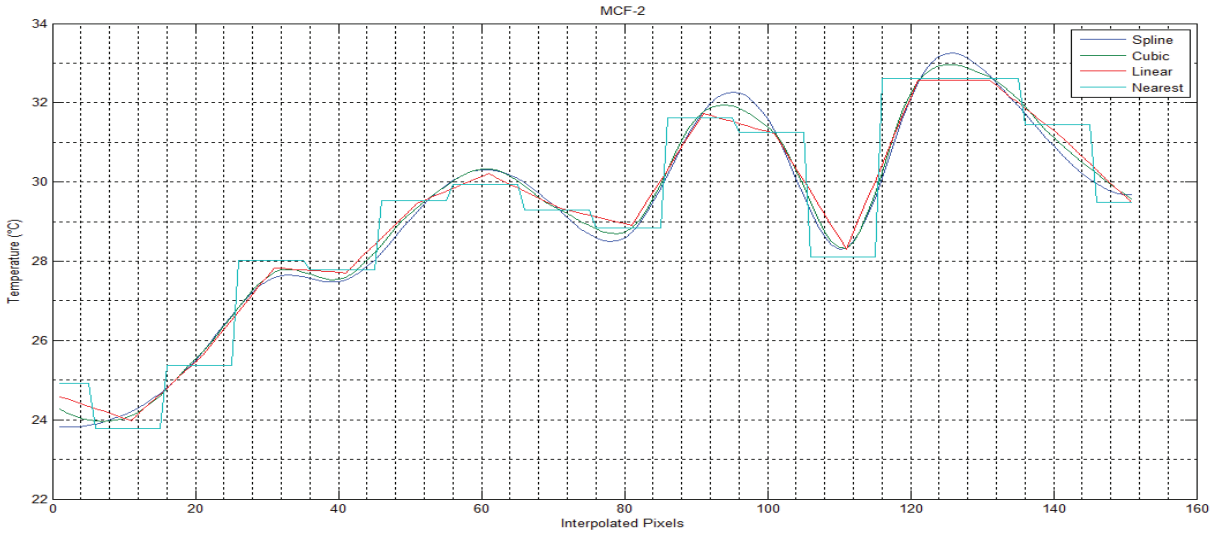
MCF-2
Spline
Cubic
Linear
Nearest
Temperature (°C)
Interpolated Pixels

(b)

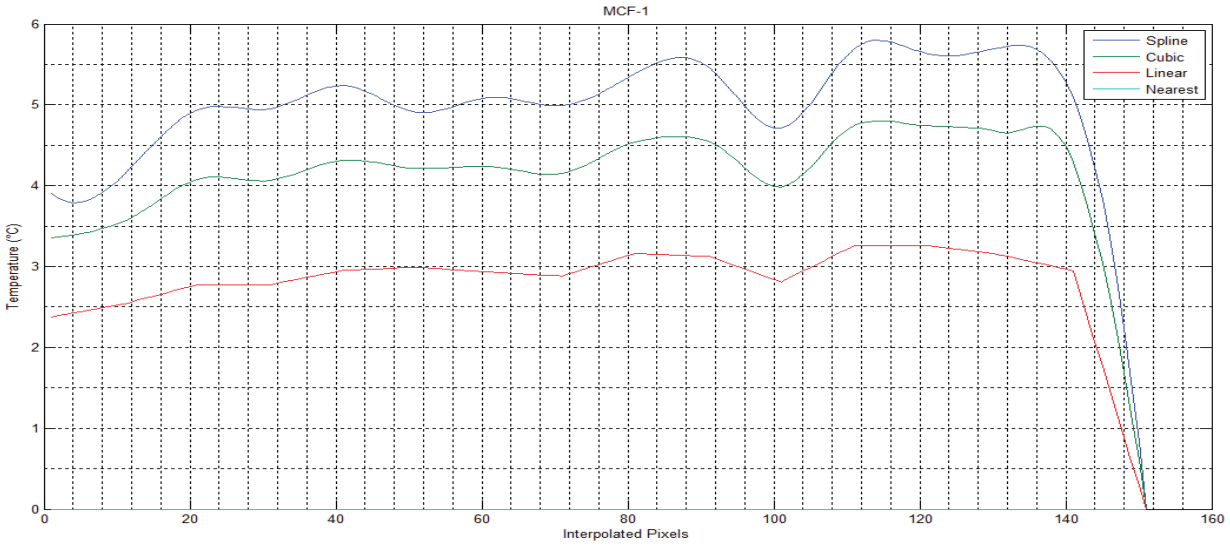
MCF-1
Spline
Cubic
Linear
Nearest
Temperature (°C)
Interpolated Pixels

(c)

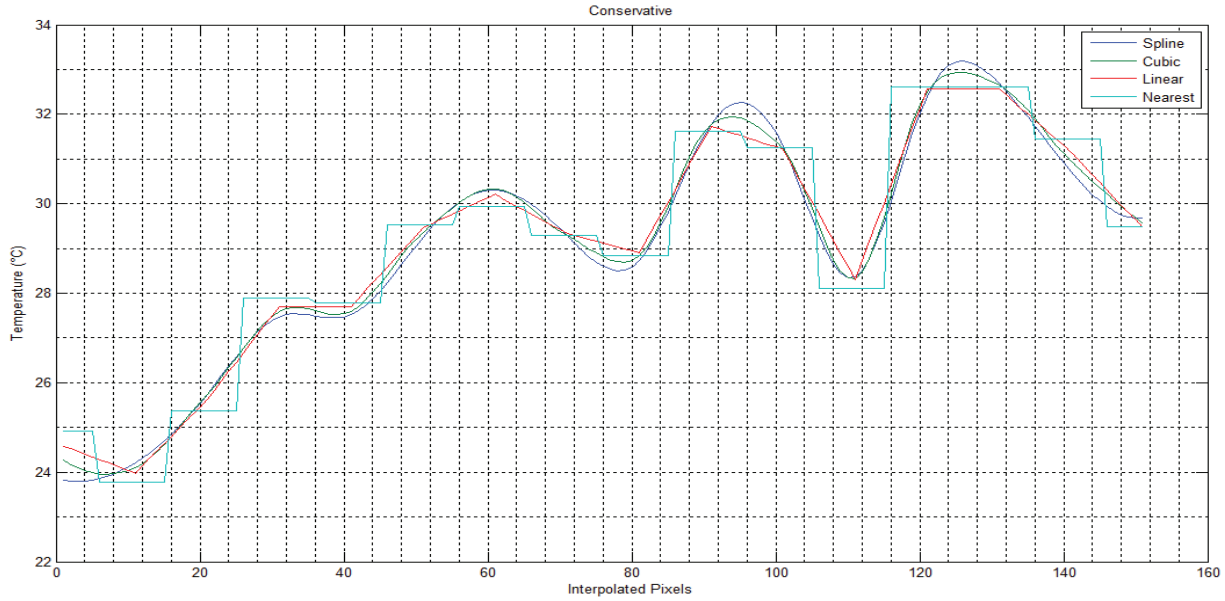

(d)

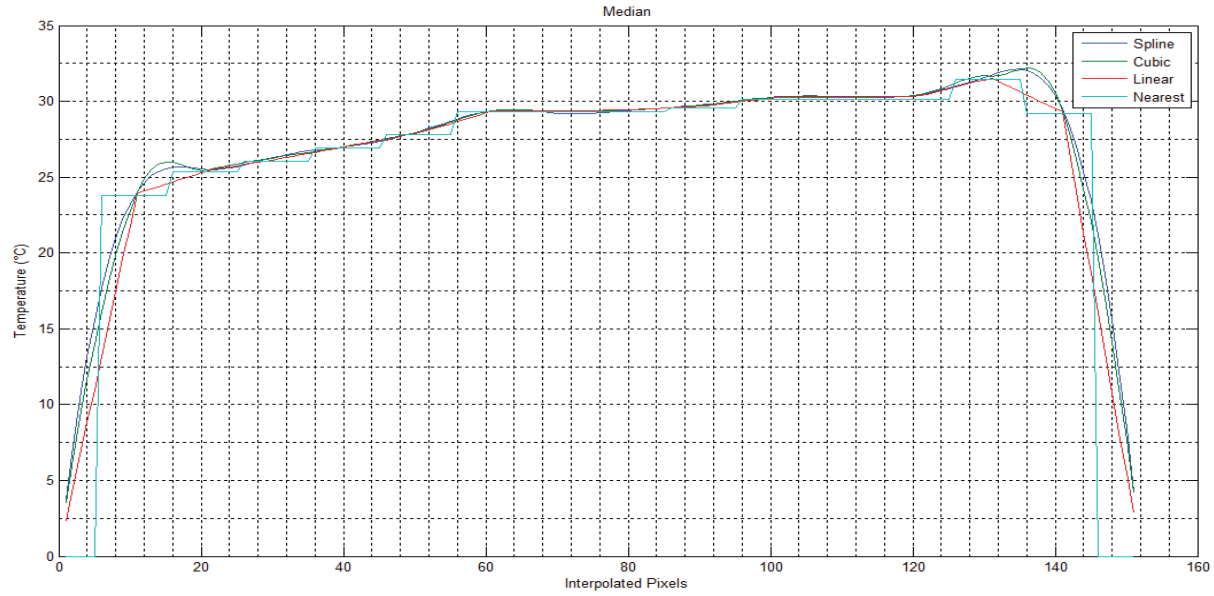

(e)

Figure 9. Thermal response of interpolated row-27 with different proposed filters.

Table 1. Data table of Figure 9a

	MCF3											
	Min	**Min2**	**Max1**	**Max2**	**Max3**	**DF1**	**DF2**	**DDF1**	**D1**	**D2**	**DDF2**	**DDF**
Spline	28.9	30	32.9	32.7	32.8	3.93	3.74	0.18	2.65	2.72	0.07	0.71
Cubic	28.9	30	32.9	32.7	32.8	3.93	3.74	0.18	2.65	2.72	0.07	0.72
Linear	28.9	30	32.9	32.7	32.8	3.93	3.74	0.18	2.65	2.72	0.07	0.71
Nearest	28.9	30	32.9	32.7	32.8	3.93	3.74	0.18	2.65	2.72	0.07	0.71

Table 2. Data table of Figure 9b

	MCF2											
	Min	**Min2**	**Max1**	**Max2**	**Max3**	**DF1**	**DF2**	**DDF1**	**D1**	**D2**	**DDF2**	**DDF**
Spline	29	30.1	32.9	32.7	32.7	3.91	3.72	0.19	2.61	2.65	0.04	0.14
Cubic	29	30.1	32.9	32.7	32.7	3.91	3.72	0.19	2.61	2.65	0.04	0.14
Linear	29	30.1	32.9	32.7	32.7	3.91	3.72	0.19	2.61	2.65	0.04	0.14
Nearest	29	30.1	32.9	32.7	32.7	3.91	3.72	0.19	2.61	2.65	0.04	0.14

Table 3. Data table of Figure 9c

	MCF1											
	Min	**Min2**	**Max1**	**Max2**	**Max3**	**DF1**	**DF2**	**DDF1**	**D1**	**D2**	**DDF2**	**DDF**
Spline	29.5	29	31	33.1	34.2	1.55	3.65	2.11	4.08	5.21	1.13	0.1
Cubic	29.5	29	31	33.1	34.2	1.55	3.65	2.11	4.08	5.21	1.13	0.1
Linear	29.5	29	31	33.1	34.2	1.55	3.65	2.11	4.08	5.21	1.13	0.1
Nearest	29.5	29	31	33.1	34.2	1.55	3.65	2.11	4.08	5.21	1.13	0.1

Table 4. Data table of Figure 9d

	Conservative											
	Min	**Min2**	**Max1**	**Max2**	**Max3**	**DF1**	**DF2**	**DDF1**	**D1**	**D2**	**DDF2**	**DDF**
Spline	28.9	30	32.9	32.7	32.8	3.91	3.73	0.19	2.63	2.72	0.09	0.49
Cubic	28.9	30	32.9	32.7	32.8	3.91	3.73	0.19	2.63	2.72	0.09	0.49
Linear	30.8	30.2	32.5	32.8	33.5	1.74	1.97	0.23	2.55	3.29	0.73	0.5
Nearest	30.8	30.2	32.5	32.8	33.5	1.74	1.97	0.23	2.55	3.29	0.73	0.5

Table 5. Data table of Figure 9e

	Median											
	Min	**Min2**	**Max1**	**Max2**	**Max3**	**DF1**	**DF2**	**DDF1**	**D1**	**D2**	**DDF2**	**DDF**
Spline	29.9	31.2	30.2	31.4	32.5	0.23	1.46	1.23	0.19	1.33	1.14	0.08
Cubic	29.9	31.2	30.2	31.4	32.5	0.23	1.46	1.23	0.19	1.33	1.14	0.08
Linear	29.9	31.2	30.2	31.4	32.5	0.23	1.46	1.23	0.19	1.33	1.14	0.08
Nearest	29.9	31.2	30.2	31.4	32.5	0.23	1.46	1.23	0.19	1.33	1.14	0.08

shows the contrast related to 'D1' and 'D2'. In the end 'DDF' Show the overall contrast result, which are relate to 'DDF1' and 'DDF2'. The data collected separately with different filters and four different interpolating techniques so, the data values show clearly for each method of interpolation with different filters in the data tables, which given below. When we compare the contrast result of Table 1 to Table 5 so, it is clearly evident that the contrast of Sp-line is much greater than Cubic, Linear and Nearest as well as the contrast result of MCF-3 is greater than other filters where Median filter gives very low contrast.

Figure-10 shows the comparison of contrast of proposed MCF-3, MCF-2, MCF-1, Conservative and Median Filter with respect to Sp-line, Cubic, linear and nearest techniques of interpolation. Here, we can clearly see that the contrast of MCF-3 is much better than the other filters where the Median filter gives low contrast as well as we can also see that the Sp-line method of interpolation works best as compare to Cubic, linear and nearest, where the nearest neighboring method of interpolation gave poor results as compare to others.

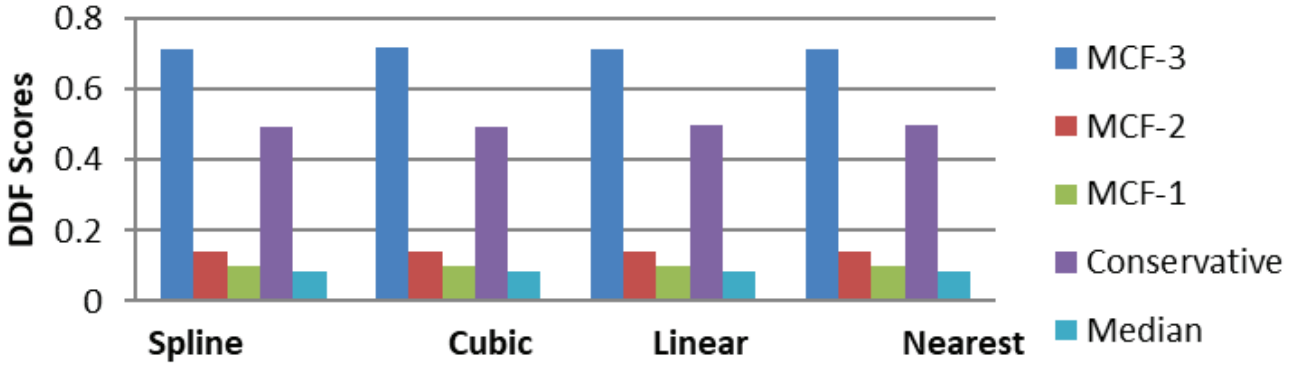

Figure 10. Comparison of contrast.

CONCLUSION

In this work, we gathered daily data values for Pakistan's upper atmosphere from the Synoptic TOA and surface fluxes and clouds (SYN) Ed4A, a data product of Clouds and the Earth's Radiant Energy System (CERES). This study aims to explore the quantification of infrared flux through exploratory data analysis. Using the results from the infrared data, we construct and analyze the thermal images. We demonstrated that, when compared to other interpolation techniques, the Sp-line method produced the best results, whereas the closest method produced subpar results. In addition to developing the Conservative and Median Filters, we employed the three suggested Modified Conservative Filters (MCF), namely MCF-1, MCF-2, and MCF-3. We found that, in comparison, our suggested Modified Conservative Filters – 3 (MCF-3) produces the greatest outcomes, while Median Filters did not produce results that were suitable. Therefore, thermal images of Modified Conservative Filters – 3 (MCF-3) are far superior to others. To improve the infrared array, use several enhancing approaches. The suggested data has much noise factors, but we make an effort to reduce them by using various filters that have been developed and suggested. We used Modified Conservative Filters – 3 (MCF-3) to assist us eliminate a lot more noise components. With the aid of various datasets, we may apply these methods for a plethora of additional uses. By creating more sophisticate filtering algorithms, in the future the noise factor will decreased. The thermal images produced by the Median Filter in this case were entirely blurry. Another question is why does the median filter fail so miserably in this case? The noise factors increased as the image size increased as we were improving the thermal images. Thus, the topic of how to improve thermal imaging without raising noise levels remains for the future.

AUTHORSHIP CONTRIBUTIONS

Authors equally contributed to this work.

DATA AVAILABILITY STATEMENT

The authors confirm that the data that supports the findings of this study are available within the article. Raw data that support the finding of this study are available from the corresponding author, upon reasonable request.

CONFLICT OF INTEREST

The author declared no potential conflicts of interest with respect to the research, authorship, and/or publication of this article.

ETHICS

There are no ethical issues with the publication of this manuscript.

STATEMENT ON THE USE OF ARTIFICIAL INTELLIGENCE

Artificial intelligence was not used in the preparation of the article.

REFERENCES

[1] Frank, Michalsky J. Solar and infrared radiation measurements. 2nd ed. Michigan: Taylor & Francis Group; 2020.

[2] Zhang H, Rao P, Xia H, Weng D, Chen X, Li Y. Modeling and analysis of infrared radiation dynamic characteristics for space micromotion target recognition. Infrared Phys Technol 2021;116. [CrossRef]

[3] Ozaki Y, Huck C, Tsuchikawa S, Engelsen SB. Near-infrared spectroscopy: Theory, spectral analysis, instrumentation, and applications. Singapore: Springer; 2021. [CrossRef]

[4] Rogalski A. Infrared and terahertz detectors. 3rd ed. Warsaw: Taylor & Francis Group; 2019. [CrossRef]

[5] Hou F, Zhang Y, Zhou Y, Zhang M, Lv B, Wu J. Review on infrared imaging technology. Sustainability 2022;14:2. [CrossRef]

[6] Coakley JA, Yang P. Atmospheric radiation. Wiley-VCH Verlag; 2014.
[7] MathWorks. MATLAB and Simulink for Engineered Systems Available at: www.mathworks.com Accessed on Feb 13, 2025.
[8] Rao J, Zheng S, Yang Y. Integrating supercomputing and artificial intelligence for life science. Patterns 2022;3:100653. [CrossRef]
[9] Verovkina G. Research in the interpolation representations of stochastic processes in the two types of interpolation knots. Eureka Phys Eng 2017;2:3–8. [CrossRef]
[10] Gonzalez RC, Woods RE, Eddins SL. Digital image processing using MATLAB. 2nd ed. New Delhi: McGraw Hill Education Pvt Ltd; 2010.
[11] Gajalakshmi N, Karunanithi S. Cubic convolution and osculatory interpolation for image analysis. Int J Creat Res Thoughts 2021;9:836–842.
[12] Pennucci TT. Frequency-dependent template profiles for high-precision pulsar timing. Astrophys J 2018;871. [CrossRef]
[13] McAndrew A. A computational introduction to digital image processing. 2nd ed. Melbourne: CRC Press; 2016. [CrossRef]
[14] Qidwai U, Chen CH. Digital image processing: An algorithmic approach with MATLAB. New York: CRC Press; 2010.
[15] Lyu X. Recent progress on infrared detectors: Materials and applications. Highlights Sci Eng Technol 2022;27:191–200. [CrossRef]
[16] Li Y, Zhou H, Li T, Wang Y, Liu Y, Wang Y. CMOS-compatible 8×2 thermopile array. Sens Actuators A Phys 2010;161:120–126. [CrossRef]
[17] Gonzalez LIL, Troost M, Amft O. Using a thermopile matrix sensor to recognize energy-related activities. In: 3rd Int Conf Sustain Energy Inf Technol (SEIT 2013); 2013. [CrossRef]
[18] Reimers M, Kolkwitz B, Beck D, Sarma M, Heinzel C, Lang W, et al. Steel integrated IR thermopile array for characterizing grinding processes. Procedia Eng 2016;168:1568–1572. [CrossRef]
[19] Wang HJ, Liu MM, Shi CC. The design of MLX90621 based intelligent lighting control system. In: Int Conf Comput Netw Commun Technol (CNCT 2016); 2016. [CrossRef]
[20] Melexis. Datasheet IR16×4. Available at: https://datasheet4u.com/datasheets/Melexis/MLX90620/1093410 Accesed on Sep 16, 2016.
[21] Ruminski D, Palczewska G, Nowakowski M, Zielińska A, Kefalov VJ, Komar K, et al. Two-photon microperimetry: Sensitivity of human photoreceptors to infrared light. Biomed Opt Express 2019;10:4551–4567. [CrossRef]
[22] El-Azazy MM. Infrared spectroscopy principles, advances, and applications. London: IntechOpen; 2019. [CrossRef]
[23] Visconti G. Fundamentals: Radiation in the atmosphere. New York: Springer; 2016. [CrossRef]
[24] Rogalski A. History of infrared detectors. Opto Electron Rev 2008;20:279–308. [CrossRef]
[25] Waele ATAM. Basic operation of cryocoolers and related thermal machines. J Low Temp Phys 2011;164:179–236. [CrossRef]
[26] Yousufzai UA, Khan AA, Dania S, Siraj A, Dildar M. Wireless transmission of solar panel energy with the help of mutual induction. Sigma J Eng Nat Sci 2023;41:192–199. [CrossRef]
[27] Gonzalez LIL, Troost M, Amft O. Using a thermopile matrix sensor to recognize energy related activities in offices. Procedia Comput Sci 2013;19:678-685. [CrossRef]
[28] Kramer R, Tighe R. Thermomechanics and infrared imaging. In: Inverse problem methodologies and mechanics of additive and advanced manufactured materials. Society for Experimental Mechanics. Proceedings of the 2021 Annual Conference on Experimental and Applied Mechanics. Conference Proceedings of the Society for Experimental Mechanics Series 2021. [CrossRef]
[29] Wang J. Indoor infrared optical wireless communications: Systems and integration. United Kingdom: Taylor & Francis Group; 2020. [CrossRef]
[30] Laurie G, Klein R, Vandegrift K. Infrared photography: Digital techniques for artistic images. 2nd ed. 2020.
[31] Vavilov V, Burleigh D. Infrared thermography and thermal nondestructive testing. Switzerland: Springer Nature; 2020. [CrossRef]
[32] Tournie E, Cerutti L. Mid-infrared optoelectronics: Materials, devices, and applications. London: Elsevier Ltd; 2020.
[33] Klijn ME, Hubbch J. Application of ultraviolet, visible, and infrared light imaging in protein-based biopharmaceutical formulation characterization and development studies. Eur J Pharm Biopharm 2021;165:319–336. [CrossRef]
[34] Zhao C, Zhang L, Zhang Y. All-sky longwave radiation modelling based on infrared images and machine learning. Build Environ 2023;238. [CrossRef]
[35] Xu M, Chen X, Bu X, Cao Y, Sun Q. Research on attitude measurement compensation technology under the influence of solar infrared radiation interference. Infrared Phys Technol 2022;123. [CrossRef]